VOL. 23, NO. 3, 2024, 38-44
elektrika.utm.my
ISSN 0128-4428

ELEKTRIKA
Journal of Electrical Engineering

Thickness-Dependent Electrical Simulation of Ternary Layer-by-Layer Organic Solar Cell

Nithyaganeshan Thamotharan[1], **Suhana Mohamed Sultan**[1*], **Nurul Ashikin Abdul Kadir**[1] and **Amirjan Nawabjan**[1]

[1]Faculty of Electrical Engineering, Universiti Teknologi Malaysia, 81310 UTM Skudai, Johor, Malaysia.

[*]Corresponding author: suhanasultan@utm.my

Abstract: Recently, researchers have been interested in incorporating a third component into the active layer of organic solar cells (OSC). Introducing a third component aims to improve the efficiency of light absorption, charge separation, and transport within the solar cell. It is widely observed that varying active layer thicknesses result in different device competencies due to the behaviour of charge transportation and charge collection in such volume morphology of active layer. This paper incorporated layer-by-layer (LbL) devices based on BTR-Cl as donor and IT-2Cl as acceptor with Y6 acceptor as a third component in the active layer. These devices had been electrically characterized using organic and hybrid material nano (OghmaNano) simulation tool. A thickness ranging between 40 nm and 100 nm of each material in the active layer was evaluated in this simulation. This simulation shows the current-voltage (I-V) characteristics for ternary LbL OSC devices at various thicknesses. The short circuit current density (J_{sc}), open circuit voltage (V_{oc}), and fill factor (FF) for each device's active layer thickness were also provided. At a thickness ratio of 50:60:50 nm (BTR-Cl to Y6 to IT-2Cl) and 100 mW cm^{-2}, AM1.5 incident solar radiance, the maximum attainable efficiency, 12.1%, was found.

Keywords: OSC, LbL, ternary devices, heterojunction devices, OghmaNano

Article History: received 30 May 2024; accepted 10 November 2024; published 30 December 2024

1. INTRODUCTION

Organic solar cells (OSCs) were discovered in 1974 by Heeger et al. Since then, OSCs have emerged as a possible alternative to standard inorganic solar cells due to their ecologically benign nature and limitless solar energy potential. The discovery of innovative acceptor and donor materials, interfacial materials for improved charge-carrier collection, and optimization of phase-separation morphology all contribute to notable improvements in the PCE of OSCs, which have already reached 19% [1].

The photoactive or active layer is the actual layer that converts light energy to electrical energy in an OSC. Three general architectures of the active layer are used: bulk-heterojunction (BHJ), layer-by-layer (LbL) and pseudo-LbL. The active layer architecture used in this simulation-based research is LbL. The LbL OSC was first developed by Tang in 1986, and the PCE could only reach 1% [2]. This was because most classical organic semiconductors had low exciton lifetime and restricted exciton diffusion lengths between 5 and 20 nm. Recent studies on the exciton diffusion length of non-fullerene acceptors have identified a wide range of new state-of-the-art acceptors that exhibit surprisingly long exciton diffusion lengths from 20 to 47 nm [3, 4]. This opens up a new window opportunity to study LbL OSCs. LbL OSC has some advantages over their BHJ counterpart, as it is more straightforward and facilitates optimization. The most notable advantage of LbL OSC is charge separation at the interface between layers, leading to better efficiency in converting sunlight into electricity.

In recent years, researchers have been incorporating a third component into the active layer of BHJ OSCs. Adding a third component increases the solar cell's light absorption, charge separation, and transport efficiency [5-7]. A few researchers have applied this method in LbL OSCs. Ren et al. 2020 demonstrated over 13 % and 16 % PCE for PBDB-T-SF/IT-4F:FBR and PM6/Y6:FBR ternary LbL system [8]. In 2023, Zhou et al. reported another ternary LbL system with a PCE approaching 18% [9]. This shows that the LbL method for ternary devices is a viable strategy for improving the efficiency of OSCs.

It is commonly known that varied active layer thicknesses, leading to different device capabilities because of how charge transportation and collection behave in such active layer volume morphologies. The common procedure to find the optimal thickness for maximum device efficiency is by varying the active layer thickness in experiments. Typically, the optimal thickness of the donor and acceptor in binary LbL devices is represented by thickness or weight ratio. Finding the optimum thickness of donors and acceptors in ternary LbL devices can be much more challenging than their binary counterparts. This is because in ternary LbL devices, charge transportation and collection behaviour is affected by either two donors and an acceptor or a donor and two acceptors.

This simulation using Oghma Nano aims to study how the electrical characteristics of ternary LbL OSC are

related to the thickness of the donor and acceptors in its active layer. In this study, the Y6 acceptor was added as a third component in the active layer of an LbL device based on BTR-Cl as a donor and IT-2Cl as an acceptor. The solar cell's performance was significantly influenced by the thickness of its donor and acceptors in the active layers, which is related to optimal optical path length for light absorption. An experiment may be designed to fabricate highly efficient ternary LbL OSC using the simulation's results in less time and cost.

2. THEORETICAL EQUATIONS

2.1 Short Circuit Current Density, J_{sc}

Short circuit current density, J_{sc} is the current per unit area. The J_{sc} can be derived from equation (1) which represents the relationship between J_{sc} and short circuit current, I_{SC} [11, 12]. The I_{SC} is the total current generated when the solar cell is short-circuited, which can be derived from equation (2).

$$J_{sc} = \frac{I_{sc}}{A} \tag{1}$$

$$I_{SC} = qG\left(L_n + L_p\right) \tag{2}$$

where A is the surface area of the layer, G is the generation rate, q is the elementary charge $(1.6 \times 10^{-19} C)$, L_n and L_p are the diffusion lengths for electron and hole.

The short circuit current density J_{sc} can be calculated theoretically as an integral over the incident light's wavelength range, taking into account the solar spectrum and the solar cell's quantum efficiency from equation (3) [12, 13].

$$J_{sc} = q \int_{\lambda_1}^{\lambda_2} b_s(\lambda) QE(\lambda) d\lambda \tag{3}$$

where q is the elementary charge $(1.6 \times 10^{-19} C)$, λ is the wavelength of light, λ_1 and λ_2 are the lower and higher wavelength limits of the integration, denoting the spectral range that the solar cell responds to, $b_s(\lambda)$ is the incident photon flux density and $QE(\lambda)$is the quantum efficiency (QE) of the cells at a given wavelength. QE is the ratio of the amount of photons of a certain energy incident to the amount of carriers collected at the electrode.

2.2 Open circuit voltage, V_{oc}

Open circuit voltage is determined from equation (4), which is derived from the Shockley diode equation [13]

$$V_{oc} = \left(\frac{nkT}{q}\right) \ln\left[\left(\frac{J_{sc}}{J_0}\right) + 1\right] \tag{4}$$

where n is the ideality factor, J_0 the dark saturation current density, q the electronic charge and T the absolute temperature.

2.3 Fill Factor, FF

The efficiency with which a solar cell transforms sunlight into electrical power is indicated by its fill factor (FF). It is defined as the ratio of the maximum power output of the solar cell to the product of the open-circuit voltage (V_{oc}) and short circuit current density (J_{sc}). The FF is determined from equation (5)

$$FF = \frac{P_{max}}{V_{oc} \times J_{sc}} \tag{5}$$

where FF is the fill factor and P_{max} is the maximum power output of the solar cell.

2.4 Power Conversion Efficiency, PCE

The PCE evaluates how effectively a solar cell converts incoming sunlight into usable electrical power. PCE is calculated by comparing the electrical power output of the solar cell to the power of the incident sunlight. The higher the PCE, the more efficient the solar cell converts sunlight into electricity. PCE can be calculated from equation (6) [5].

$$\eta = \frac{Jsc \times Voc \times FF}{P_{in}} \tag{6}$$

where η is the PCE and $P_{in} = 100$ mW cm^{-2} is the incident solar radiance at AM1.5 used in this simulation.

3. SIMULATION PARAMETERS

The device's simulated structure is shown in Figure 1 (a). The device comprises seven layers, three of which contribute as the active layer. The other four layers consist of transparent top electrode, electron transport layer (ETL), hole transport layer (HTL) and back electrode. The transparent top and back electrodes used in this simulation are Indium tin oxide (ITO) and silver (Ag), which serve as the cathode and anode, respectively. The ETL aids in extracting and transporting photogenerated electron carriers while also serving as hole blocking layer. The HTL facilitates the movement of positive carriers while inhibiting the movements of electrons. The ETL and HTL used in this simulation are Zinc oxide (ZnO) and Molybdenum oxide (MoO_x).

The active layer is the layer that carries out the process of conversion of light energy to electrical energy. The active layer comprises two non-fullerene small molecule acceptors and a small molecule donor sandwiched on top of each to form a ternary LbL OSC. The small molecule acceptors and IT-2Cl and Y6, while the small molecule donor is BTR-Cl. These small molecules were chosen and sandwiched in the active layer based on the molecules' highest occupied molecular orbital and lowest unoccupied molecular orbital energy level alignment, as shown in Figure 1 (b).

The normalized absorption coefficient of BTR-Cl, Y6 and IT-2Cl is shown in Figure 1 (c). These small molecules were also chosen based on their absorption spectrum to ensure a minimal absorption spectrum overlap between the three small molecules while increasing the overall absorption spectrum of the OSC. The absorption spectrum of BTR-Cl is between 440 nm and 690 nm, with its peak absorption at 583 nm. The absorption spectrum of Y6 is between 610 nm and 900 nm, with its peak absorption at 818 nm. The absorption spectrum of IT-2Cl is between 580 nm and 800 nm, with its peak absorption at 732 nm.

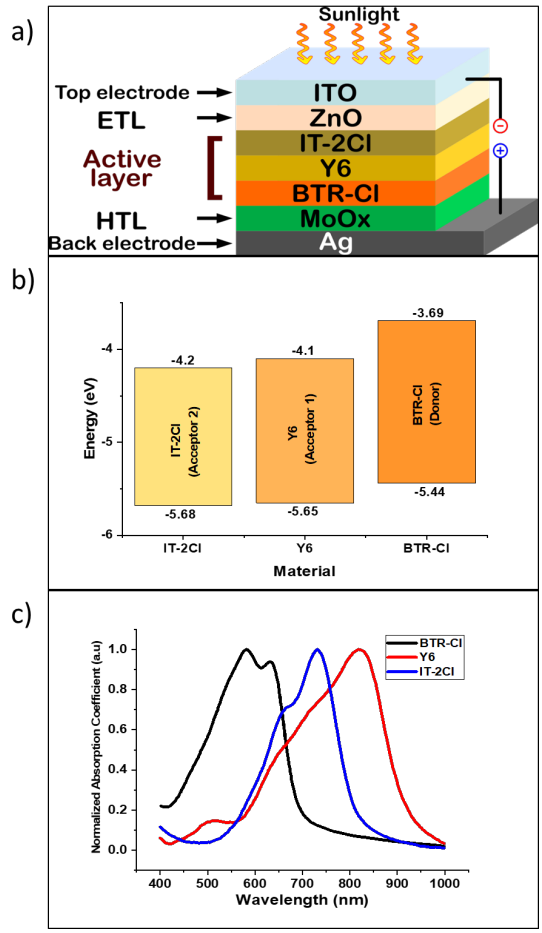

Figure 1. a) Ternary LbL OSC structure for OghmaNano simulation. b) The energy level diagram of donor and acceptors. c) Normalized absorption coefficient of BTR-Cl, Y6 and IT-2Cl

Table 1. Thickness of transparent top electrode, electron transport layer, hole transport layer and back electrode.

Layer	Material	Thickness (nm)
Transparent top electrode	ITO	100
ETL	ZnO	30
HTL	MoO_x	10
Bottom electrode	Ag	100

The thickness of the active layer was manipulated by varying the thickness of the donor and acceptors using OghmaNano software under 100 mW cm^{-2}, AM1.5G incident solar radiance. First, the device was simulated with varying IT-2Cl thicknesses of 40 nm, 60 nm, 80 nm and 100 nm, respectively, at a fixed Y6 and BTR-Cl thickness at 50 nm. Next, the simulation was repeated with varying Y6 thicknesses of 40 nm, 60 nm, 80 nm and 100 nm, respectively, at a fixed IT-2Cl and BTR-Cl thickness at 50 nm. Similarly, the third simulation was repeated with varying BTR-Cl thicknesses of 40 nm, 60 nm, 80 nm and 100 nm, respectively, at a fixed IT-2Cl and Y6 thickness at 50 nm. The material and thickness for the transparent top electrode, electron transport layer, hole transport layer and back electrode were kept constant throughout the three simulations, as shown in Table 1.

4. RESULTS AND DISCUSSION

Figure 2 shows the I-V characteristics of the simulated device under 100 mW cm^{-2}, AM1.5G incident solar radiance at different IT-2Cl/Y6/BTR-Cl thicknesses. The maximum current generated by the device at 1.2 V is when the thickness of IT-2Cl is at 100nm, Y6 at 50 nm and BTR-Cl at 50 nm. Figure 2 (a) shows that the current generated increases as the thickness of IT-2Cl increases. This is because increasing the thickness of IT-2Cl results in more material available to absorb incident photons. This can lead to increased photon absorption and, consequently, higher generation of excitons and current [14].

However, Figure 2 (b) shows a very slight decrease in the current generated as the thickness of Y6 is increased. This indicates the photon absorption of Y6 is reduced as the thickness increases. The active layer materials in LbL devices are deposited in separate layers, which causes the position closer to the incident photon to minimize the incident photon available to the layers below it if the materials have overlapping absorption spectrum [8]. Despite that, the decrease in the current generated as the thickness of Y6 increases is only slightly affected by its overlapping absorption spectrum with IT-2Cl. This is because Y6 has a wider absorption spectrum, which does not overlap with other materials in the active layer, as shown in Figure 1 (c).

In Figure 2 (c), similar to Y6, an observable decrease in current generated as the thickness of BTR-Cl increases is observed due to limited photons available for absorption due to overlapping absorption spectrum with Y6 and IT-2Cl. This indicated that with limited photons available for absorption, increasing the thickness only increases the path length that charge carriers must traverse through the material. This can lead to a higher probability of charge carriers undergoing scattering events, encountering traps, or recombining, contributing to increased effective resistance within the device [15]. To conclude, the layer with the most significant influence on the I-V characteristic is IT-2Cl, followed by Y6 and BTR-Cl.

Figure 3 (a) shows the influence of thickness on short circuit current density, J_{sc}, for the three configurations of OSCs. The short circuit current density rises when the active layer is thicker because it absorbs more light and produces more electron-hole pairs [16]. However, the short circuit current density, J_{sc}, for all three configurations shows a lowered value as the thickness of one material increases in the active layer. The highest value of J_{sc} is observed by 15.41 mA/ cm^2 at the thickness of Y6 at 60 nm, with IT-2Cl and BTR-Cl at 50 nm. This shows that excessively increasing the thickness of a material in active layer may also result in increased charge recombination and hinder efficient charge extraction, decreasing the short circuit current density [17].

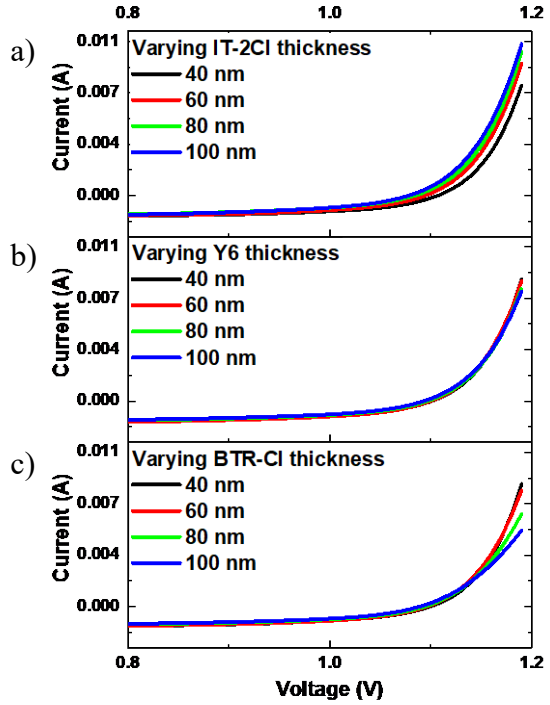

Figure 2. I-V characteristics with varying thicknesses of a) IT-Cl. b) Y6. c) BTR-Cl.

Figure 3 (b) shows the influence of varying material thickness in the active layer on open circuit voltage, V_{oc} for the three configurations of OSCs simulated. It is observed that the V_{oc} decreases as the thickness of the layer increases for all three configurations. Increasing the thickness of IT-2Cl gave a more significant negative effect on its V_{oc} than increasing the thickness of Y6 and BTR-Cl. The highest value of V_{oc} obtained is 1.107 V with IT-2Cl at 40 nm and BTR-Cl and Y6 at 50 nm. Generally, increasing the thickness of the active layer can enhance light absorption, leading to a higher generation of electron-hole pairs and, hence, a larger open circuit voltage [18]. However, the result obtained in this simulation for the three configurations shows otherwise. Researches have found that by increasing the thickness of the active layer, researchers can enhance light absorption and increase the number of charge carriers generated [19].

On the other hand, decreasing the thickness can reduce charge recombination and improve charge extraction [19]. This reason explains the decreases in V_{oc} as the layer thickness increased in all three configurations simulated. The thickness of each material in the active layer of an OSC influences the morphology and interface between layers in the active layer. This can affect the energy level alignment, charge transfer kinetics, and overall device performance [20].

Figure 3 (c) shows the effect of active layer thickness on PCE for all three configurations simulated. The highest PCE was 12.1% obtained with Y6 at 60 nm and BTR-Cl and IT-2Cl at 50 nm. The configuration with varying thicknesses of Y6 yields a higher PCE when its thickness is more than the other two materials when compared to the configurations with varying thicknesses of BTR-Cl and IT-2Cl. This is because Y6 has a broader absorption spectrum when compared to the other two materials. This also indicates that to fully utilize the wide absorption spectrum of Y6, the thickness of IT-2Cl, which is positioned above Y6 in this LbL OSC, has to be manipulated to be thinner while still retaining its usefulness in the device since both materials have a partially overlapping absorption spectrum.

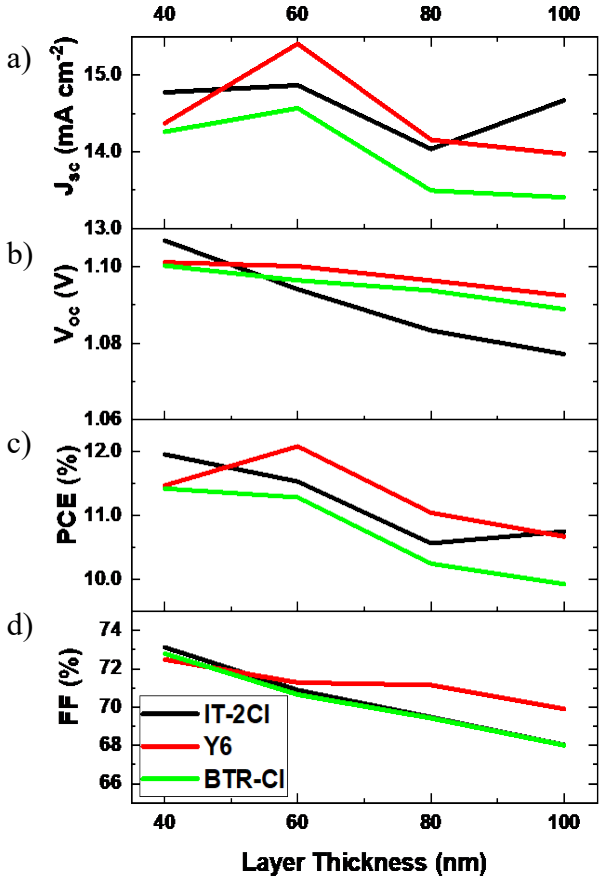

Figure 3. Variation of key performance metrics with different thickness ratios of small molecules: a) Short circuit current density (J_{sc}), b) Open circuit voltage (V_{oc}), c) Power conversion efficiency (PCE), and d) Fill factor (FF)

Figure 3 (d) shows the influence of the varying material thickness in the active layer on the fill factor, FF, for the three configurations of OSCs simulated. An obvious decrease in FF as a layer's thickness increases is observed for all three configurations. The highest value of FF obtained is 73%, with IT-2Cl at 40 nm and BTR-Cl and Y6 at 50 nm. Varying the thickness of a material in the active layer causes the shunt resistance of the device to change. When the thickness of a layer is reduced, the shunt resistance is also reduced, which can improve charge collection and reduce recombination losses, resulting in a higher fill factor [21]. On the other hand, it should also be noted that increasing the thickness of the active layer can also enhance light absorption, leading to a higher number of excitons generated and ultimately resulting in a higher fill factor [22]. Tables 2, 3 and 4 show the electrical simulation results under 100 mW cm$^{-2,}$ AM1.5G incident solar radiance at different IT-2Cl/Y6/BTR-Cl thicknesses on key ternary LbL OSC performance metrics.

Table 5 compares OSC active layer architecture, PCE, fabrication and optimization complexity, and significant contributions of this work and others. When comparing the other three works with this study, critical differences in performance and complexity arise. While this work achieved a PCE of 12% using a ternary LbL OSC with trilayer architecture where donor and acceptors are deposited in separate layers, the other studies all reported higher efficiencies.

Ren et al. (2020) reported two bilayer devices where the donor is deposited in one layer while the two acceptors are deposited as a BHJ in a separate layer. Ren et al. (2020) achieved 13% and 16% PCE using the bilayer architecture, which is higher than this work's 12%. However, while the fabrication complexity was similar (moderate), the optimization in Ren's work was significantly more difficult. Despite this challenge, their architecture excelled in efficient charge generation and transport, offering a technical edge.

Zhou et al. (2023) reported the highest PCE at 18% using a ternary BHJ architecture. Though the fabrication process was more accessible than the others, the optimization was complex due to the ternary BHJ architecture. Zhou's work achieved a significantly higher efficiency due to the large donor-acceptor interface that the BHJ provides compared to this work's 12%, highlighting the potential of the BHJ structure for pushing efficiency boundaries. In summary, while this work is more straightforward to optimize and involves a simpler architecture, the other studies offer higher efficiencies but with added complexity in optimization.

Table 2. The Electrical simulation at different thicknesses of IT-2Cl at a light intensity of 100mW/cm²

Thickness of IT-2Cl (nm)	J_{sc} (mA cm^{-2})	V_{oc} (V)	PCE (%)	FF (%)
40	14.778	1.107	11.961	73.123
60	14.870	1.094	11.534	70.893
80	14.039	1.083	10.566	69.474
100	14.674	1.077	10.752	68.022

Table 3. The Electrical simulation at different thicknesses of Y6 at a light intensity of 100mW/cm²

Thickness of Y6 (nm)	J_{sc} (mA cm^{-2})	V_{oc} (V)	PCE (%)	FF (%)
40	14.375	1.101	11.474	72.490
60	15.412	1.100	12.087	71.286
80	14.159	1.096	11.046	71.155
100	13.973	1.092	10.671	69.906

Table 4. The Electrical simulation at different thicknesses of BTR-Cl at a light intensity of 100mW/cm²

Thickness of BTR-Cl (nm)	J_{sc} (mA cm^{-2})	V_{oc} (V)	PCE (%)	FF (%)
40	1.100	1.101	11.425	72.800
60	1.096	1.100	11.287	70.648
80	1.094	1.096	10.249	69.425
100	1.089	1.092	9.930	68.010

Table 5. Comparison of organic solar cell architectures, power conversion efficiencies (PCE), fabrication complexities, and key advantages across different studies.

Work	Active Layer Architecture and material	PCE (%)	Complexity		Significance/ Advantages
			Fab*	Opt*	
This Work	BTR-Cl/Y6/IT-2Cl(Trilayer)	12%	Mod*	Easy	-Simple architecture
Ren et al. (2020)	PBDB-T-SF/IT-4F:FBR (bilayer)	13%	Mod*	Diff*	-Efficient charge generation. -Efficient charge transport and collection properties
Ren et al. (2020)	PM6/Y6:FBR (bilayer)	16%	Mod*	Diff*	-Efficient charge generation -Efficient charge transport and collection properties
Zhou et al. (2023)	PM6:BPR-SCl:BTP-eC9 (BHJ)	18%	Easy	Com*	-Large donor-acceptor interface -High PCE

*Fab – Fabrication
*Opt -Optimization
*Mod-Moderate. Diff-Difficult Com – Complex

5. CONCLUSION

Using OghmaNano simulation software, the electrical properties of ternary LbL OSCs at various BTR-Cl/Y6/IT-2Cl thickness ratios were examined. The numerical modelling used in this software, reveals that the highest efficiency achieved 12.1% with Y6 at 60 nm and both BTR-Cl and IT-2Cl at 50 nm. In general the change in thickness of one small molecule shows a significant effect in the optical absorption of other small molecules in the active layer. As both IT-2Cl and Y6 have a somewhat overlapping absorption spectrum, the thickness of IT-2Cl, which is positioned above Y6 in this ternary LbL OSC, must be adjusted to be thinner while maintaining its utility in the device to utilize the broad absorption spectrum of

Y6 fully. On the other hand, a thinner BTR-Cl, which acts as a donor in the active layer, reduces effective resistance within the device and increases its efficiency.

ACKNOWLEDGMENT

This work was supported by the UTM Fundamental Research Grant with UTM cost centre no. Q.J130000.3823.23H25.

REFERENCES

[1] T. Walia Binte and U. Ashraf, "A review of progress and challenges in the research developments on organic solar cells," Materials Science in Semiconductor Processing, vol. 163, p. 107541, 2023, doi: https://doi.org/10.1016/j.mssp.2023.107541.

[2] C. W. Tang, "Two-layer organic photovoltaic cell," Applied Physics Letters, vol. 48, no. 2, pp. 183-185, 1986, doi: 10.1063/1.96937.

[3] Y. Firdaus et al., "Long-range exciton diffusion in molecular non-fullerene acceptors," Nature Communications, vol. 11, no. 1, p. 5220, 2020/10/15 2020, doi: 10.1038/s41467-020-19029-9.

[4] T. H. Lee et al., "Organic Planar Heterojunction Solar Cells and Photodetectors Tailored to the Exciton Diffusion Length Scale of a Non-Fullerene Acceptor," Advanced Functional Materials, vol. 32, no. 51, p. 2208001, 2022, doi: https://doi.org/10.1002/adfm.202208001.

[5] K. S. Ram and J. Singh, "Over 20% Efficient and Stable Non-Fullerene-Based Ternary Bulk-Heterojunction Organic Solar Cell with WS2 Hole-Transport Layer and Graded Refractive Index Antireflection Coating," Advanced Theory and Simulations, vol. 3, no. 6, p. 2000047, 2020, doi: https://doi.org/10.1002/adts.202000047.

[6] X. Minghai et al., "Ternary organic solar cells with improved efficiency and stability enabled by compatible dual-acceptor strategy," Organic Electronics, vol. 96, p. 106227, 2021, doi: https://doi.org/10.1016/j.orgel.2021.106227.

[7] C. Xianjie et al., "18.02% Efficiency ternary organic solar cells with a small-molecular donor third component," Chemical Engineering Journal, vol. 424, p. 130397, 2021, doi: https://doi.org/10.1016/j.cej.2021.130397.

[8] M. Ren et al., "High-Performance Ternary Organic Solar Cells with Controllable Morphology via Sequential Layer-by-Layer Deposition," ACS Applied Materials \& Interfaces, vol. 12, no. 11, pp. 13077-13086, 2020, doi: 10.1021/acsami.9b23011 , note = PMID: 32079401.

[9] Z. Hao et al., "Approaching 18% efficiency of ternary layer-by-layer polymer solar cells with alloyed acceptors," Chemical Engineering Journal, vol. 462, p. 142327, 2023, doi: https://doi.org/10.1016/j.cej.2023.142327.

[10] X. Ma et al., "Efficient Ternary Polymer Solar Cells with Two Well-Compatible Donors and One Ultranarrow Bandgap Nonfullerene Acceptor," Advanced Energy Materials, vol. 8, 01 2018, doi: 10.1002/aenm.201702854.

[11] O. Pang-Leen and I. Levitsky, "Organic/IV, III-V Semiconductor hybrid solar cells," Energies, vol. 3, 03 2010, doi: 10.3390/en3030313.

[12] N. Yusop, F. p. Chee, A. Alias, A. B. Abd Rahman, and A. I. Abdul Rani, "Electrical Simulation for Different Thickness Ratio of PCBM and PTAA in Bilayer Organic Solar Cells," ASM Science Journal, vol. 13, p. 2020, 09 2020, doi: 10.32802/asmscj.2020.sm26(2.12).

[13] M. Nath, S. Chakraborty, E. V. Johnson, A. Abramov, P. Roca i Cabarrocas, and P. Chatterjee, "Factors limiting the open-circuit voltage in microcrystalline silicon solar cells," EPJ Photovolt., vol. 2, p. 20101, 2011. [Online]. Available: https://doi.org/10.1051/epjpv/2011025.

[14] K. Sreedhar Ram, H. Mehdizadeh-Rad, D. Ompong, D. D. Y. Setsoafia, and J. Singh, "Characterising Exciton Generation in Bulk-Heterojunction Organic Solar Cells," Nanomaterials, vol. 11, no. 1, p. 209, 2021. [Online]. Available: https://www.mdpi.com/2079-4991/11/1/209.

[15] N. Syafiqa, G. Bablu Kumar, D. Pratap Kumar, "Organic-inorganic PTAA-SiGe transparent optical materials performance analysis for photo device applications," Optical Materials, vol. 147, p. 114768, 2024, doi: https://doi.org/10.1016/j.optmat.2023.114768. C. Fuei Pien, K. A. Mohamad, and S. Ismail,

[16] E. Naveen Kumar, K. Raju, B. B. Beenarani, H. A. Mohammed, K. Mun-Kyeom, and Z, "Recent developments in perovskite materials, fabrication techniques, band gap engineering, and the stability of perovskite solar cells," Energy Reports, vol. 11, pp. 1171-1190, 2024, doi: https://doi.org/10.1016/j.egyr.2023.12.068.

[17] K. Kim and B. Kim, "Rhodanine-Based Non-Fullerene Acceptors for Organic Solar Cells with a High Open-Circuit Voltage of 1.07 V," Journal of Flexible and Printed Electronics, vol. 2, no. 1, pp. 119-143, 2023, doi: 10.56767/jfpe.2023.2.1.119.

[18] H. Rakib, S. Sawrab, U. Md. Shihab, H. Md. Manjurul, M. Hayati, and B. Mohammad Ruhul Amin, "Effect of various layers on improving the photovoltaic efficiency of Al/ZnO/CdS/CdTe/Cu2O/Ni solar cells," Journal of Alloys and Metallurgical Systems, vol. 4, p. 100041, 2023, doi: https://doi.org/10.1016/j.jalmes.2023.100041.

[19] M. H. Mohammadi, M. Eskandari, and D. Fathi, "Design of optimized photonic-structure and analysis of adding a SiO2 layer on the parallel CH3NH3PbI3/CH3NH3SnI3 perovskite solar cells," Scientific Reports, vol. 13, no. 1, p. 15905, 2023/09/23 2023, doi: 10.1038/s41598-023-43137-3.

[20] C. Wang et al., "Recent Progress in Covalent Organic Frameworks for Cathode Materials," Polymers, vol. 16, no. 5, p. 687, 2024. [Online]. Available: https://www.mdpi.com/2073-4360/16/5/687.

[21] K. An et al., "Mastering morphology of non-fullerene acceptors towards long-term stable organic solar cells," Nature Communications, vol. 14, no. 1, p. 2688, 2023/05/10 2023, doi: 10.1038/s41467-023-38306-x.

[22] M. Li et al., "Trap-Filling of ZnO Buffer Layer for Improved Efficiencies of Organic Solar Cells," (in English), Frontiers in Chemistry, Original Research vol. 8, 2020-May-26 2020, doi: 10.3389/fchem.2020.00399.